Analysis, Characterization and Minimization of IPMSMs Cogging Torque with Different Rotor Structures

M. Caruso, A. O. Di Tommaso, S. Emma and R. Miceli, *Member, IEEE*

Department of Energy, Information Engineering and Mathematical Models - University of Palermo, Viale delle Scienze, Building nr. 9, 90128 Palermo, Italy. e-mail: massimo.caruso16@unipa.it, antoninooscar.ditommaso@unipa.it, salvatore.emma@gmail.com, rosario.miceli@unipa.it

***Abstract*—This paper presents the analysis, characterization and comparison of the cogging torque components generated by five different IPMSM rotor structures. More in detail, an IPMSM model (named IPMSM1), which is derived from a commercial geometry, is analyzed by using a Finite Element Method (FEM) approach. Then, four other IPMSM models, which are obtained by modifying the IPMSM1 rotor structure and by maintaining the same stator configuration, are proposed and analyzed. From the obtained simulation results, the cogging torque components for each structure are determined and compared. From this comparison, a significant cogging torque decrease is occurring for the modified geometries, without affecting the values of the generated torque. Furthermore, a meaningful relationship between the peak values of the cogging torque and the gradients of the flux density around the neutral area is reported and discussed. Therefore, simple structure modifications applied to the rotor geometry can bring significant improvements in terms of motor performances and cogging torque reduction.**

***Index Terms*—Cogging torque, IPMSM, permanent magnets, FEM analysis, optimization.**

I. Introduction

DURING the last two decades, the scientific interest towards permanent magnet synchronous machines (PMSMs) has been significantly increased, as well as their application fields. As a matter of fact, these machines are widely used in several electrical drive applications, improving the development of automated systems in both the industrial and automotive fields. This improvement is due to the great advantages introduced by PMSMs in comparison with other type of electrical machines: higher efficiency, power factor, torque/weight and power/current ratios are only some examples of the better performances achieved by this type of machine. In addition, the motor does not need brushes for the excitation current, because the excitation flux is generated by the permanent magnets (high energy NdFeB and SmCo PMs). Therefore, the power losses mainly occur in the stator.

Nowadays, the scientific research in the field of brushless machines and their drives is mainly directed towards the improvement of some of their characteristics, such as torque/weight and torque/moment of inertia ratios [1], efficiency [2] and torque pulsation [3]. The latter is a very critical phenomenon for specified applications (e.g. servo drives) and it is composed by two main components: the ripple torque and the cogging torque. The ripple torque is determined by the interaction between the flux density generated by the permanent magnets and the space harmonics produced by the stator currents. The cogging torque is caused by the interaction between the stator teeth and the permanent magnets located inside the rotor. This component significantly decreases the motor torque performances, introducing acoustic disturbances, vibrations and mechanical stress. In addition, for low-speed electrical drives, the overall generated torque is more affected by the cogging torque component, because the resonant frequency of the motor is in the same order of magnitude of that of the cogging harmonics, highly reducing the accuracy of the speed and position control loops.

This work analyzes and compares the cogging torque generated by five different rotor structures, derived from a commercial IPMSM. It will be demonstrated that, with a simple modification applied in the rotor geometry, significant improvements in terms of motor performances and relevant

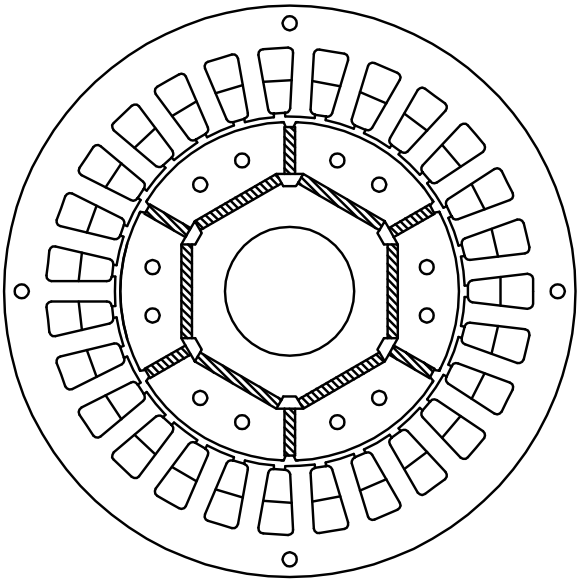

Figure 1. Cross section of the IPMSM1 structure.

978-1-4673-6785-1/15/$31.00 © 2015 IEEE

cogging torque reduction can be appreciated, without the use of pole skewing techniques or other more complex methods [4]–[7].

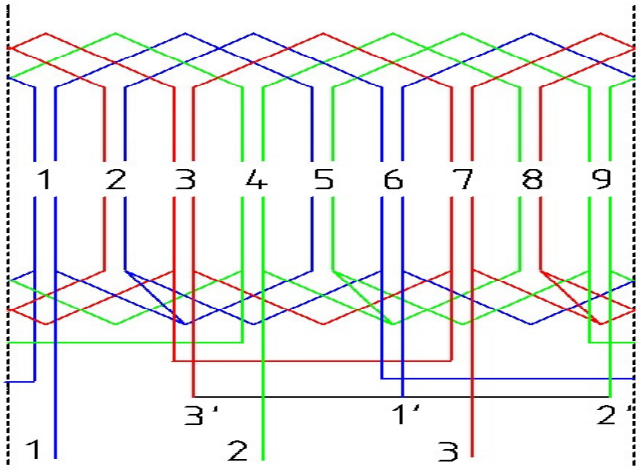

Figure 2. Basic winding scheme of the three-phase IPMSM (27 slots, 6 poles).

More in detail, this paper is structured as follows:

- In Section II, an IPMSM geometry, which has been discussed in [1] is presented and the related FEM analysis is carried out, in order to determine the values of the cogging torque.
- In Section III, the rotor structure of the previously described model is modified in four possible geometries, but maintaining the same stator configuration. This allows to evaluate the IPMSM performances only in dependence of the rotor structure. The FEM analysis is, then, carried out for each of the so obtained structures and the related results are reported.
- In Section IV, for each model described in Section III, the FEM results are discussed. From the comparison of the related cogging torque components, a significant reduction of the cogging torque is achieved, optimizing, therefore, the motor performances.

II. IPMSM Structure and FEM Analysis

The motor geometry taken as reference is named IPMSM1 and its cross section is shown in fig. 1. The motor structure is a six-poles machine, whose NdFeB permanent magnets are mounted in order to produce a magnetic flux in the tangential and in the radial direction. Moreover, the stator winding is a three-phase, star, double layer and shortened pitch, located into 27 slots. The number of slots per pole per phase is equal to 1.5. The stator and rotor cores are realized with iron laminates, whose magnetic permeability in the linear region and electrical conductivity are equal to μ_r=14800 and σ=10.44 MS/m, respectively.

The base winding scheme of the proposed model is shown in fig. 2, whereas a visual description of the different parts of the motor is depicted in fig. 3.

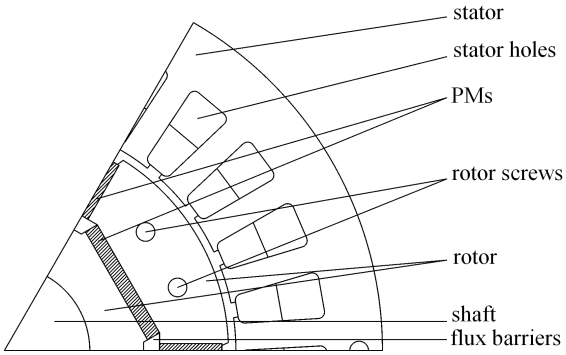

Figure 3. Angular cross-section of the motor with the description of the different parts.

It is well known that the cogging torque phenomenon and its related effects have been extensively analyzed in literature, from analytical approaches [8], [9] to finite element models [10]. In this study, a FEM approach has been preferred to analytical methods. For this purpose, the FEMM 4.2 software has been used and three process phases have been followed:

1) *pre-processing*, which is characterized by the definition of the motor geometry, by the selection of the type of materials and by the assignment of the related boundary conditions.
2) *solution*, in which the FEM solution of the problem is determined and the flux density field values in the nodes of the finite elements are calculated.
3) *post-processing*, where the solutions in terms of scalar or vector quantities are analyzed, displayed and managed.

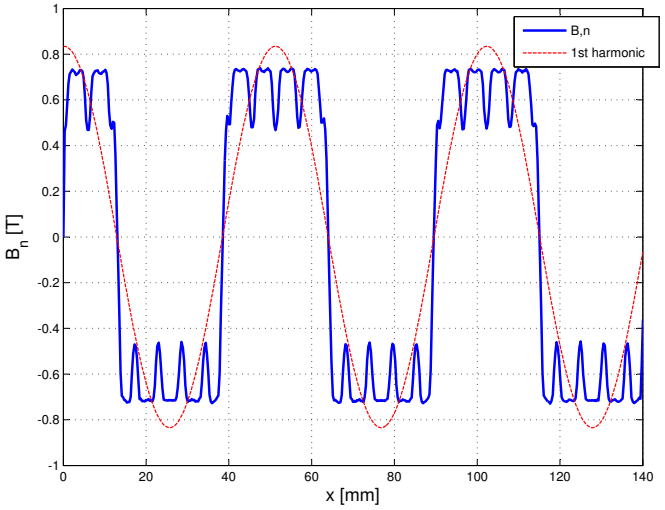

Figure 4. Radial component of the flux density as a function of the air gap length.

Thus, the FEMM4.2 has allowed to determine:

- the density plot of the flux density field;
- the spatial distribution of the radial component of the flux density, B_n, as function of the coordinate x (measured on the circumference passing through the middle of the air-gap), which is shown in fig. 4;

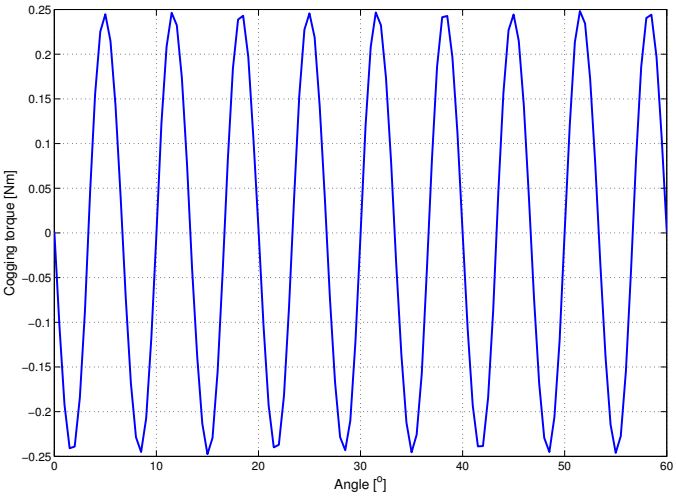

Figure 5. Calculated values of the cogging torque.

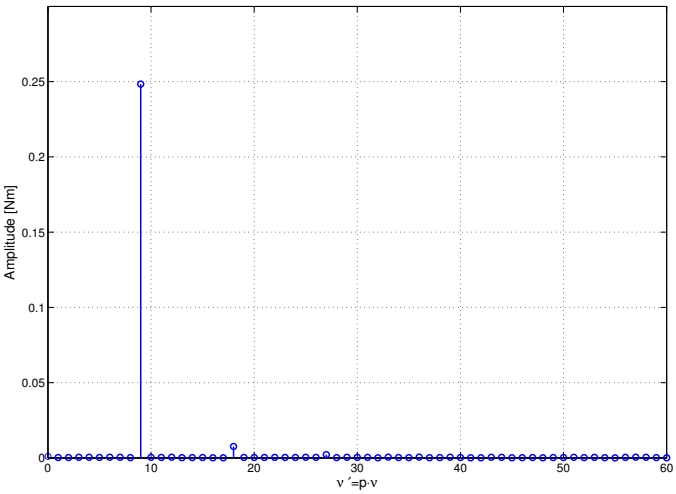

Figure 6. Harmonic spectrum of the cogging torque for the IPMSM1 model.

- the flux produced by a single pole and its average value;
- the generated torque as a function of the angular position of the rotor;
- the cogging torque trend, shown in fig. 5;
- the harmonic spectrum of the cogging torque, which is reported in fig. 6.

The cogging torque has been calculated by simulating a rotation of the rotor by four tooth pitches without the supply of the driving currents, according to [11]. Therefore, 9 periods of the cogging torque (calculated in a IPMSM sector of 60°) have been determined and the possible presence of noise, due to the discrete nature of the calculation method, has been filtered. The fundamental harmonic of the cogging torque corresponds to the 9^{th} order harmonic of the determined spectrum due to the nine complete periods contained in the 60° sector (see fig. 5).

From this FEM analysis it can be noticed that the peak value of the calculated cogging torque is equal to $\hat{T}_1$=0.2482 Nm, which is the 7.410% of the maximum value of the generated torque (see Table I).

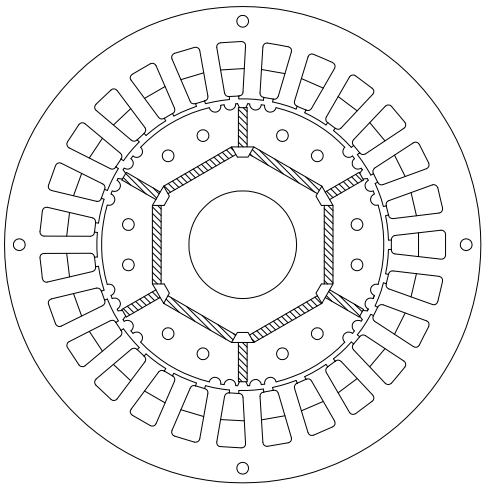

Figure 7. Cross section of the IPMSM2 structure.

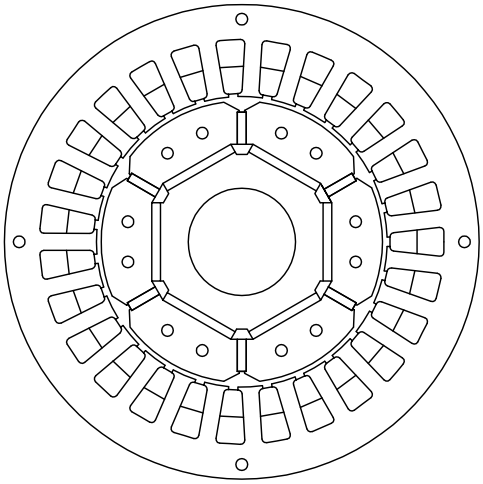

Figure 8. Cross section of the IPMSM3 structure.

III. Cogging Torque Reduction for the Proposed IPMSM Structures

In this section, the IPMSM1 rotor structure is modified in order to reduce the main cause that determines the cogging torque. As a matter of fact, this cogging torque component depends on the spatial variation of the electromagnetic energy stored in the stator slots [12]. The highest variation is detected when a tooth crosses the magnetic neutral zone, due to the fact that in this area the radial component of the flux density, B_n, reaches its maximum gradient (see fig. 4). Thus, the geometrical modifications of the IPMSM1 rotor structure are finalized to reduce this gradient, in order to bring back the trend of B_n as much as possible to the ideal case of sinusoidal distribution (see fig. 4).

Four new IPMSM rotor structures (IPMSM2, IPMSM3, IPMSM4 and IPMSM5) are here presented and described. For each model, the same IPMSM1 stator configuration is adopted. This allows to evaluate the performances of the machine only in dependence of the rotor structure modification.

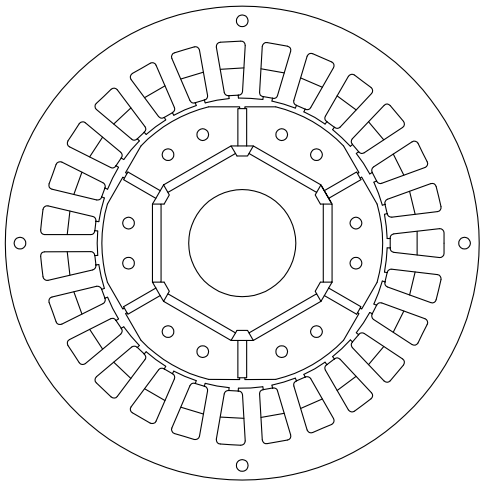

Figure 9. Cross section of the IPMSM4 structure.

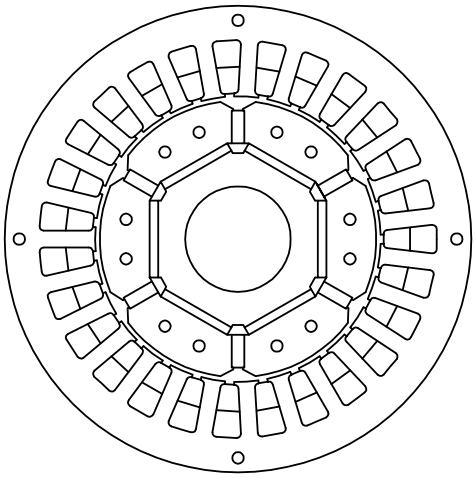

Figure 10. Cross section of the IPMSM5 structure.

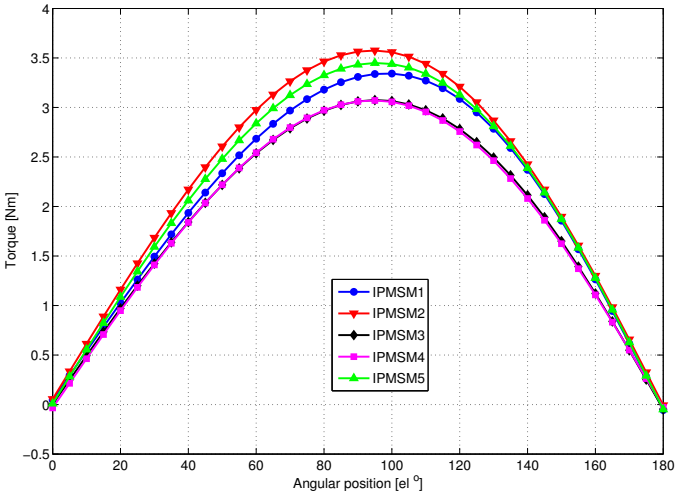

Figure 11. Torque/load angle characteristic comparison for the IPMSM structures.

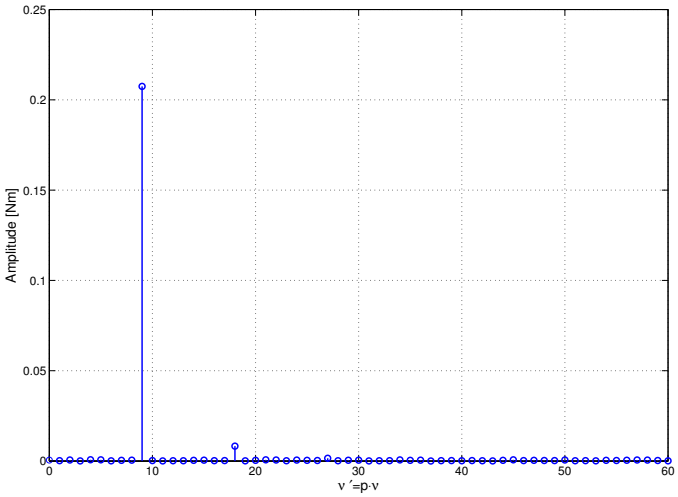

Figure 12. Harmonic spectrum of the cogging torque for the IPMSM2 model.

Firstly, the IPMSM1 rotor structure has been modified by designing longitudinal semicylindrical grooves near the neutral axis of the poles, as shown in fig. 7. The so obtained model, named IPMSM2, has been analyzed by following the same procedures described in section II.

Secondly, the IPMSM3 structure has been obtained by realizing longitudinal cuts at the ends of the poles and by reducing the length of radially mounted magnets by a quantity of 0.9 mm, as shown in fig. 8.

Thirdly, by executing tangential cuts along the edges of the poles, the IPMSM4 structure is obtained. In comparison with the IPMSM3 model, a higher length of the radially mounted magnets is achieved, as detected by looking at fig. 9.

Finally, the IPMSM5 structure has been realized by modifying the IPMSM3 model. More in detail, the thickness of the radially mounted PMs has been increased from 1.5 mm to 2.3 mm, obtaining the configuration shown in fig. 10.

IV. Results and Discussions

The data acquired from the FEM analysis previously described have been analyzed and processed for each of the proposed IPMSM models. More in detail, the torque/load angle characteristic is shown in fig. 11. From this graph it

Table I
Cogging torque harmonics and their relative percentage values, with respect to T_{max}, of each type of IPMSM (non-percentage torque values are expressed in Nm).

IPMSM nr.		1	2	3	4	5
T_{max}		3.35	3.57	3.075	3.07	3.45
ν=9	T_ν	0.2481	0.2071	0.0100	0.0172	0.0160
	T_ν% [%]	7.406	5.801	0.325	0.560	0.463
ν=18	T_ν	0.0083	0.0082	0.0005	0.0054	0.0007
	T_ν% [%]	0.248	0.230	0.0162	0.0175	0.020
ν=27	T_ν	0.0022	0.0010	0.0003	-	0.0005
	T_ν% [%]	0.066	0.028	0.009	-	0.014
$\hat{T} = \sqrt{\sum_\nu T_\nu^2}$		0.2482	0.2073	0.010	0.0180	0.0160
$\frac{\hat{T}}{T_{max}}$% [%]		7.410	5.806	0.326	0.587	0.464

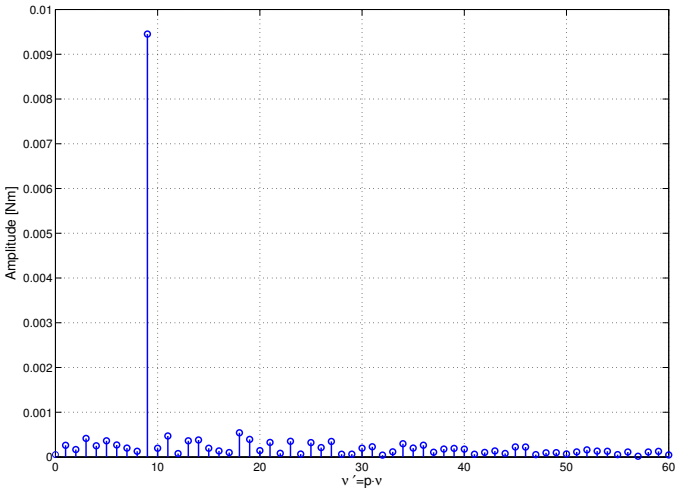

Figure 13. Harmonic spectrum of the cogging torque for the IPMSM3 model.

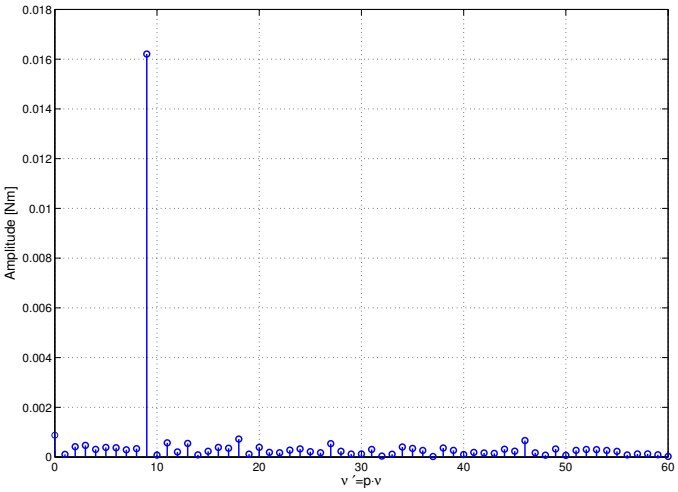

Figure 15. Harmonic spectrum of the cogging torque for the IPMSM5 model.

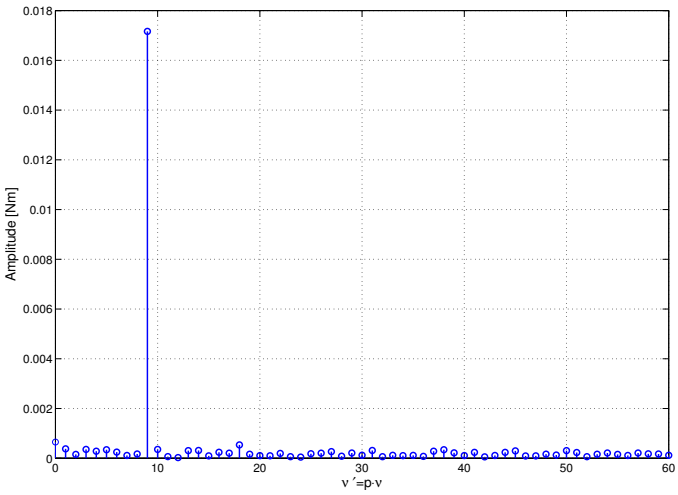

Figure 14. Harmonic spectrum of the cogging torque for the IPMSM4 model.

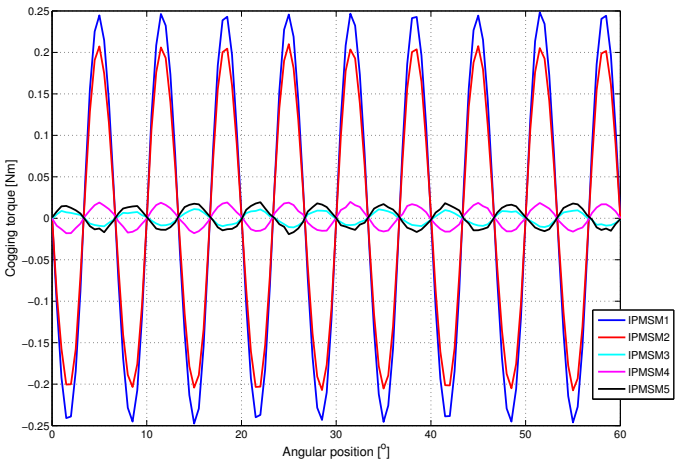

Figure 16. Cogging torque characteristics of the IPMSM structures.

can be noticed that the maximum value of generated torque is achieved by the IPMSM2 model and it is equal to 3.57 Nm for an electrical load angle of 95°. Moreover, the related harmonic spectra are shown in figs. 12, 13, 14 and 15.

The cogging torque trends of each IPMSM structure as function of the angular position of the rotor are all reported in the same graph of fig. 16. By comparing the motor performances in terms of produced cogging torque component, it can be noticed that the IPMSM2 structure did not lead to any significant change, although the overall generated torque has been increased (see fig. 11). In fact, the calculated peak value of the cogging torque is equal to $\hat{T}_2$= 0.2073 Nm (see Table I), which almost corresponds to the same value obtained for the model described in section II. On the contrary, the cogging torque peak harmonics produced by the IPMSM3, IPMSM4 and IPMSM5 structures have been considerably decreased to $\hat{T}_3$=0.010 Nm (0.326% of the maximum torque T_{max}), $\hat{T}_4$=0.018 Nm (0.587% of T_{max}) and $\hat{T}_5$=0.016 Nm (0.464% of T_{max}), respectively. However, this improvement has led to a slight reduction in terms of maximum generated torque for both the IPMSM3 and IPMSM4 models. This fact is caused by an increase of the air gap near to the neutral zone and reducing the average value of the flux density. The IPMSM5 geometry has been developed in order to compensate the effect by increasing the PM width and obtaining the maximum torque value equal to 3.45 Nm.

Thus, by analyzing the proposed configurations and the related performances characteristics, it can be stated that the IPMSM1 geometry has been modified in order to significantly decrease the cogging torque component from 7.410% to 0.326% of the maximum deliverable torque, without reducing the fundamental component of the generated torque.

Table I summarizes the values of the harmonics obtained from the FEM analysis, which have been processed in order to determine the previously mentioned cogging torque trends. The percentage values of cogging torque are determined as $T_\nu\% = {}^{T_\nu}/_{T_{max}} \cdot 100$. It is possible to notice that for the IPMSM1 model the major contribution for the cogging torque is due to the 9-th harmonic (equal to 0.2481 Nm), as for the other IPMSM structures. With regard to the IPMSM5 configuration, the percentages of the harmonics are all confined between 0.014% and 0.463% of the maximum torque, which confirms the well designed geometry of this last model.

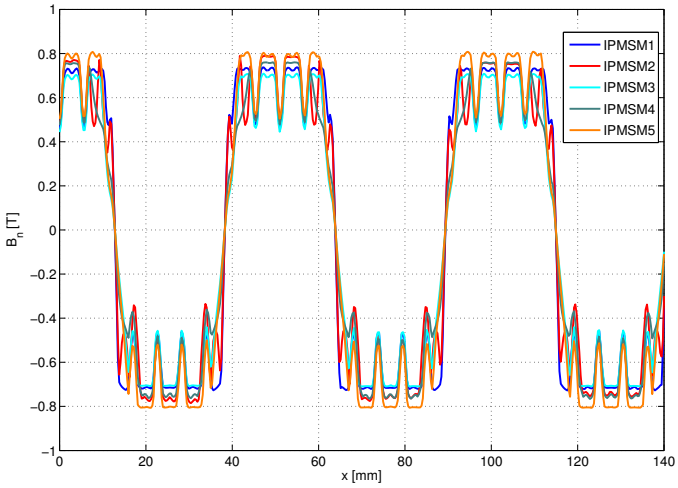

Figure 17. Comparison between the radial components of the flux density generated by the IPMSMs structures.

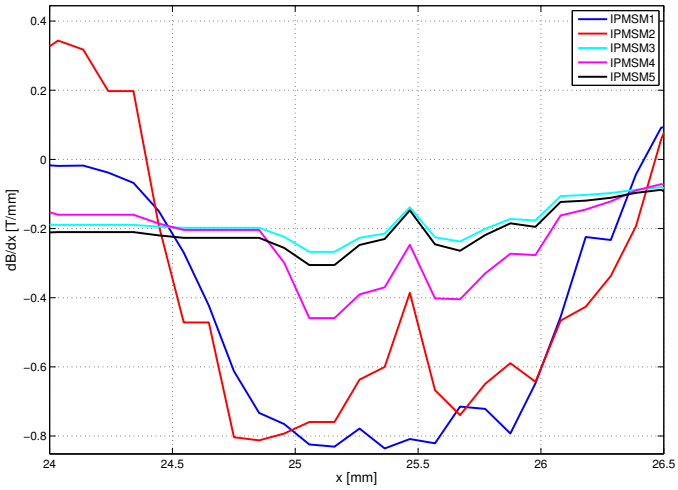

Figure 18. Comparison between the gradients of the flux density, around the q-axis region, generated by the IPMSMs structures.

Moreover, fig. 17 shows the spatial distribution of the radial component of the flux density as function of the position x measured along the mean air gap circumference. From the comparison between the related gradients around the neutral axis (quadrature axis), which are reported in fig. 18, it can be noticed that with the adoption of the IPMSM3 and IPMSM5 rotor structures the radial flux density gradient has been highly decreased, while the gradient for the IPMSM2 model is almost equal to the one determined for the IPMSM1 structure (which is significantly higher than the ideal sinusoidal case). Furthermore, a significant relationship between the gradients and the cogging torque peaks can be detected. In conclusion, by smoothly increasing the air gap near the q-axis, the cogging torque peaks can be almost reduced without resorting to pole skewing techniques and without affecting the maximum available machine torque.

V. Conclusions

This paper has presented a possible method to be adopted for the minimization of the cogging torque component in IPMSM structures. Five different machine models have been proposed and analyzed and the FEM approach has allowed the determination of the cogging torque component for each IPMSM rotor structure. From the comparison between the obtained results, it can be stated that the cogging torque component can be significantly decreased by properly modifying an IPMSM rotor structure, without significantly affecting the values of the generated torque. Furthermore, a meaningful relationship between the peak values of the cogging torque and the gradients of the flux density around the neutral area has been demonstrated.

Acknowledgments

This work was financially supported by MIUR - Ministero dell'Istruzione dell'Universita' e della Ricerca (Italian Ministry of Education, University and Research) - through FFR-2012/2013 fundings, by PON04a2_H "i-NEXT" italian research program and by SDESLab (Sustainable Development and Energy Saving Laboratory) of the University of Palermo. The Authors wish to thank all the SDESLab staff.

References

[1] M. Caruso, A. O. Di Tommaso, R. Miceli, P. Ognibene, and G. Ricco Galluzzo, "An ipmsm torque/weight and torque/moment of inertia ratio optimization," in *22th International Symposium on Power Electronics, Electrical Drives, Automation and Motion, SPEEDAM*, June 2014.

[2] M. Uddin and F. Abera, "Development of a model based efficiency optimization for ipmsm drive," in *Electrical and Computer Engineering, 2009. CCECE '09. Canadian Conference on*, pp. 837–840, May 2009.

[3] T. Jahns and W. Soong, "Pulsating torque minimization techniques for permanent magnet ac motor drives-a review," *Industrial Electronics, IEEE Transactions on*, vol. 43, pp. 321–330, Apr 1996.

[4] N. Bianchi and S. Bolognani, "Design techniques for reducing the cogging torque in surface-mounted pm motors," in *Industry Applications Conference, 2000. Conference Record of the 2000 IEEE*, vol. 1, pp. 179–185 vol.1, 2000.

[5] P. Roshanfekr, S. Lundmark, T. Thiringer, and M. Alatalo, "Torque ripple reduction methods for an interior permanent magnet synchronous generator," in *Power Electronics and Applications (EPE'14-ECCE Europe), 2014 16th European Conference on*, pp. 1–7, Aug 2014.

[6] W. Fei and Z. Zhu, "Comparison of cogging torque reduction in permanent magnet brushless machines by conventional and herringbone skewing techniques," *Energy Conversion, IEEE Transactions on*, vol. 28, pp. 664–674, Sept 2013.

[7] M. Aydin and M. Gulec, "Reduction of cogging torque in double-rotor axial-flux permanent-magnet disk motors: A review of cost-effective magnet-skewing techniques with experimental verification," *Industrial Electronics, IEEE Transactions on*, vol. 61, pp. 5025–5034, Sept 2014.

[8] M. Tavakkoli and S. Madani, "A new approach to analysis and mitigation of pm motor cogging torque," in *Industrial Electronics, 2008. IECON 2008. 34th Annual Conference of IEEE*, pp. 2003–2008, Nov 2008.

[9] X. Wang, Y. Yang, and D. Fu, "Study of cogging torque in surface-mounted permanent magnet motors with energy method," *Journal of Magnetism and Magnetic Materials*, vol. 267, no. 1, pp. 80 – 85, 2003.

[10] M. Barcaro and N. Bianchi, "Torque ripple reduction in fractional-slot interior pm machines optimizing the flux-barrier geometries," in *Electrical Machines (ICEM), 2012 XXth International Conference on*, pp. 1496–1502, Sept 2012.

[11] D. Ionel, M. Popescu, M. McGilp, T. Miller, and S. Dellinger, "Assessment of torque components in brushless permanent-magnet machines through numerical analysis of the electromagnetic field," *Industry Applications, IEEE Transactions on*, vol. 41, pp. 1149–1158, Sept 2005.

[12] G. Bramerdorfer, S. Silber, E. Marth, G. Jungmayr, and W. Amrhein, "Analytic determination of cogging torque harmonics of brushless permanent magnet machines," in *Power Electronics, Electrical Drives, Automation and Motion (SPEEDAM), 2012 International Symposium on*, pp. 60–65, June 2012.